Direct observation of sub-picosecond vibrational dynamics in photoexcited myoglobin

C. Ferrante[1], E. Pontecorvo[1] G. Cerullo[2] M. H. Vos[3] T. Scopigno[1]

[1]*Dipartimento di Fisica, Università di Roma "La Sapienza", I-00185, Roma, Italy*

[2]*IFN-CNR, Dipartimento di Fisica, Politecnico di Milano,*

P.zza L. da Vinci 32, 20133 Milano, Italy and

[3] *LOB, Ecole Polytechnique, CNRS, INSERM,*

Université Paris-Saclay, 91128 Palaiseau Cedex, France

Contents

Supplementary Information

Supplementary Materials: ***Numerical model*** -The rationale of our model is to reproduce the vibrational dynamics accounting for anharmonic effects, obtaining mode-specific temperature evolutions upon photoexcitation. To this aim, we need to account for both the population evolution and the Raman excitation profile (REP), which we extend to determine single hot band intensities.

Since population dynamics is experimentally observed as hot bands which, in turn, originate from a single coordinate anharmonicity, we introduce a Morse potential of the kind:

$$V(r) = D_e(1 - e^{-a(r-r_e)})^2$$

The distribution of non-evenly spaced levels depends on the α parameter as:

$$E_n = \left(n + \frac{1}{2}\right)\left(1 - \alpha\left(n + \frac{1}{2}\right)\right)h\nu_i \tag{1}$$

Where n labels the vibrational level and h is the Planck constant. Each vibrational mode, $\nu_i = \frac{a}{2\pi}\sqrt{\frac{2D_e}{m}}$, has in general a specific anharmonicity factor $\alpha = \frac{h\nu_i}{4D_e}$, due to the local curvature of the potential along a given vibrational coordinate. The linewidth of each vibrational contribution, depends on the life-time of the mode and on the spectral resolution (dominated by the spectral width of the RP). To reproduce the experiment at 460 nm and 440 nm RP we use $\Gamma = 12$ cm^{-1}, and $\Gamma = 15$ cm^{-1}, respectively.

A critical aspect which needs to be taken into account is the coupling between different modes[1]. This effect generates a temporal evolution of the Morse potential along a given coordinate, related to the heating of coupling modes, which results in frequency shift of both the fundamental and the hot bands transitions. We find such shifts to be correlated with the TA dynamics. For the ν_4 peak, for instance, we observe a temporal evolution (see eq. 1) with a profile similar to that of the TA at 450 nm and a maximum shift of 5.5 cm^{-1}. This effect is accounted for by eq. 1, identifying the $\nu_i(t)$ dependence with the experimentally observed dynamics of the fundamental $0 \rightarrow 1$ vibrational transition. Under off-resonance conditions, the spectral intensity evolution only depends on the population of each vibrational level, which generates a contribution of the kind:

$$L_{i,n}(\nu) = \frac{1}{2\pi}\frac{\Gamma}{(\nu - (E_{n+1} - E_n)/h)^2 + (\Gamma/2)^2}P_{i,n}(T_i(t)) \tag{2}$$

Where $P_{i,n}$ is the occupation probability of the n-th level for the vibrational mode ν_i, which tracks population dynamics, and is obtained by local temperatures corresponding to the dynamics of transient absorption (see Fig. 2). We assume indeed that the population of each vibrational mode is in thermodynamic pseudo-equilibrium, following a mode dependent Boltzmann distribution.

We now turn to the evaluation of the REP, critically relevant in view of the different resonance conditions which we explore in our experiment. We connect a given mode intensity to the temporal evolution of the absorption spectrum via the expression[2–4]:

$$REP_i(\nu_R) \propto (\overline{n}_i + 1) S_i |\phi(t, \nu_R) - \phi\left(t, \nu_R - \nu_i\right)|^2 \tag{3}$$

where ν_R is the RP wavelength, $\overline{n}$ represents the average occupation, S_i is the Franck-Condon coupling strength and $\phi(t, \nu)$ is

$$\phi(t, \nu) = \frac{1}{\pi} P \int_{-\infty}^{\infty} d\nu' \frac{A(t, \nu')}{\nu'(\nu' - \nu)} + \imath \frac{A(t, \nu)}{\nu} \tag{4}$$

being $A(t, \nu)$ the molecular absorption coefficient at a specific pump-probe time delay, t. This approach, originally developed for resonance spontaneous Raman experiments, can be extended to stimulated Raman[5].

Since we aim to reproduce the spectral intensities of the experimentally detected hot bands, we extend the REP evaluation of a given mode by shifting it over transitions starting from higher lying vibrational levels. To this purpose, we modify eq. 3 adding the energy shift $E_n - E_0$ (to compensate for the reduced energy gap to the Soret level -see fig. 5a), still using the total absorption, under the assumption that the heating of a single vibrational mode i has a negligible contribution to the $A(t, \nu)$ profile.

$$REP_{i,n}(\nu_R) \propto (n+1) |\phi\left(t, \nu_R + (E_n - E_0)\right)/h - \phi\left(t, \nu_R + (E_n - E_0)/h - \nu_i\right)|^2 \tag{5}$$

where n is the initial vibrational level involved in the Raman probing process. The analytical expression of the signal for the $i - th$ mode, which can be directly compared to the experimental Raman gain (fig. 4), finally reads:

$$RG_i(\nu, \nu_R) = \sum_{n=0}^{\infty} L_{i,n}(\nu) REP_{i,n}(\nu_R) \tag{6}$$

Since the experimental data indicate two distinct behaviours for low and high frequency modes, we used two corresponding temperature profiles associated to the TA experiment, as explained in the main text.

Notably, eq. 5 implies that, for a given mode, the optimal resonance condition can be highly selective with respect to a specific vibronic transition, as shown in fig. S3 by the large differences in the REP wavelength dependence for the $n = 0$, as opposed to the $n \neq 0$ case. By tuning the RP of the FSRRS experiment close to the maximum of (deoxy-Mb) Soret band, therefore, the fractional contribution of hot bands to the ground state transition is strongly suppressed. Conversely, by red-shifting the RP, the relative hot bands intensity can be emphasized at the expenses of the fundamental transition, despite the relatively weak vibrationally excited population.

Supplementary Discussion: ***FSRRS vs TRRS experiments*** - At variance with FSRRS experiments, TRRS[6,7] does not probe the spectroscopic response of the system for a sharply defined time delay. By changing the laser fluence, however, the average time delay between adjacent photon interactions can be conveniently controlled and, in turn, the averaged time evolution of thermal and electronic dynamics can be accessed. Hence, TRRS and FSRRS experiments are naturally related.

In Ref.[6] a TRRS experiment with low fluence excitation (50-200 photons in 10 ns) on FeOEP-2MeIm is reported. The main results is the observation of anomalous thermal relaxation between different vibrational modes. In particular, two high frequency vibrational modes (ν_4 and ν_3) act as bottleneck for the cooling process. The temperature increase vs fluence profile extracted from the experiment[6] is reported in fig S4. We can benchmark our results against this TRRS study by averaging the mode dependent temperature profile obtained by FSRRS over the average time interval between two photon interactions at a given TRRS fluence. The result is shown in fig. S4, and it corroborates the existence of different relaxation patterns for low and high frequency modes. The temporal window corresponding to the explored fluence range (10-100 MW cm^{-2}), is 50-200 ps. Hence, the slower, high frequency modes naturally display a relatively larger increase when compared to low frequencies.

A second TRRS experiment[7], performed at much larger flux ($\sim$ 1 GW/cm^2 at 420 nm, corresponding to a picosecond regime), shows an asymmetric shape of the ν_4. In the light of our FSRRS result, this feature is clearly rationalized in terms of anharmonic coupling

generating an effect similar to the one reported in the inset of our Fig.3b, but blurred over the ps timescale integrated in the TRRS experiment. This further supports our conclusion of a dynamics ruled by a vibrationally hot ground state.

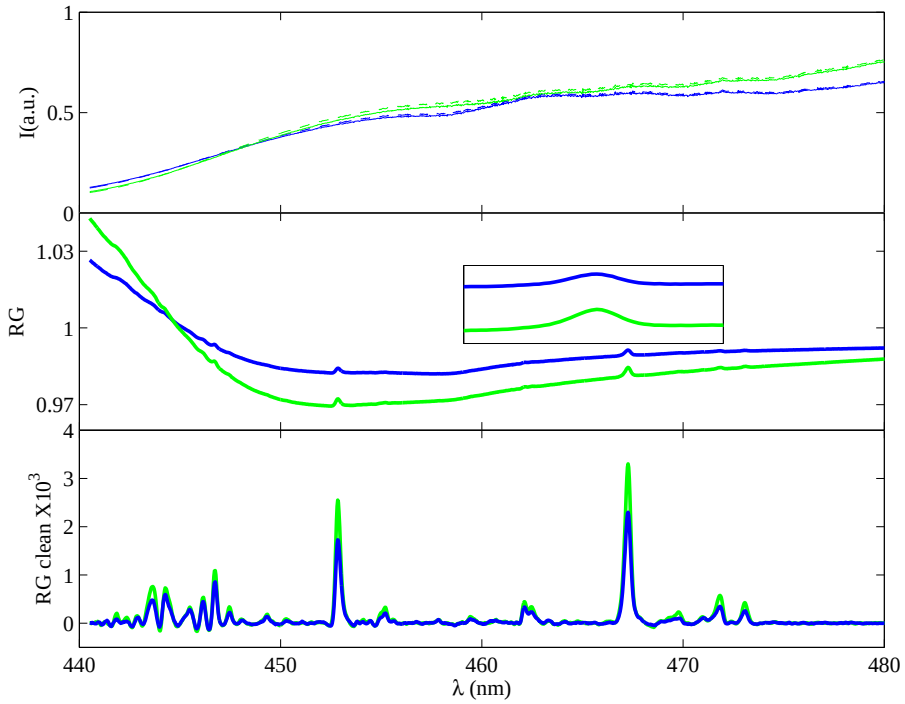

FIG. S1: **FSRRS data reduction.** FSRRS data obtained in deoxy-Mb with the RP at 440 nm for a time delay between the Actinic pump and the WLC probe equal to 0.25 ps. In the top panel we report the average of spectra obtained with (blue lines) and without (green lines) the Actinic pump. The Raman spectrum can be obtained from the ratio between the spectrum with (I_{Ron}, solid line) and without (I_{Roff}, dashed line) the RP. In the middle panel the Raman spectra with and without the Actinic pump are shown. In the inset the magnification in the range of ν_4 is shown. In the bottom panel we display the two Raman spectra after background subtraction.

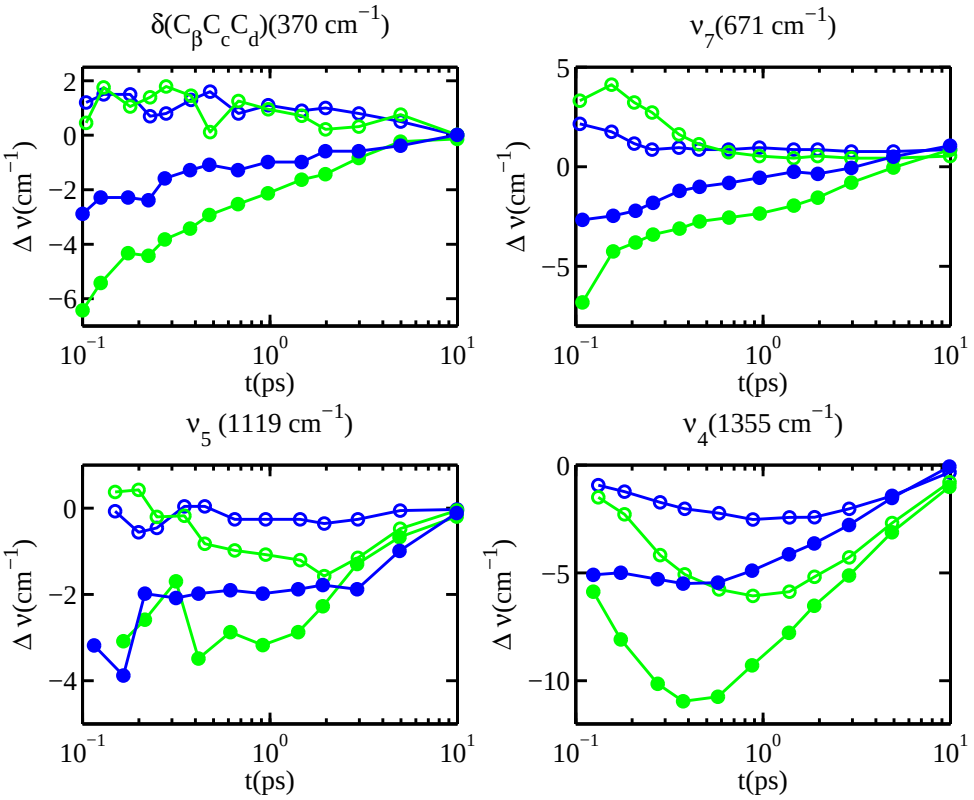

FIG. S2: **Raman shift for different FSRRS spectral lines.** Shifts in peak frequencies for different Raman modes vs time delays for 460 nm RP (filled symbols) and 440 nm RP (open symbols). MbCO and deoxy-Mb are indicated in blue and green, respectively. $\delta(C_\beta C_c C_d)$ and ν_7 profiles suggest an instantaneous heating, testified by a large red-shift at 460 nm RP, absent in the measurement with the 440 nm RP. A different scenario holds for high frequency modes (bottom panels), showing that the red-shift is delayed by 1 ps. The smaller MbCO shifts with respect to deoxy-Mb indicates a reduced heating for the ligated specie.

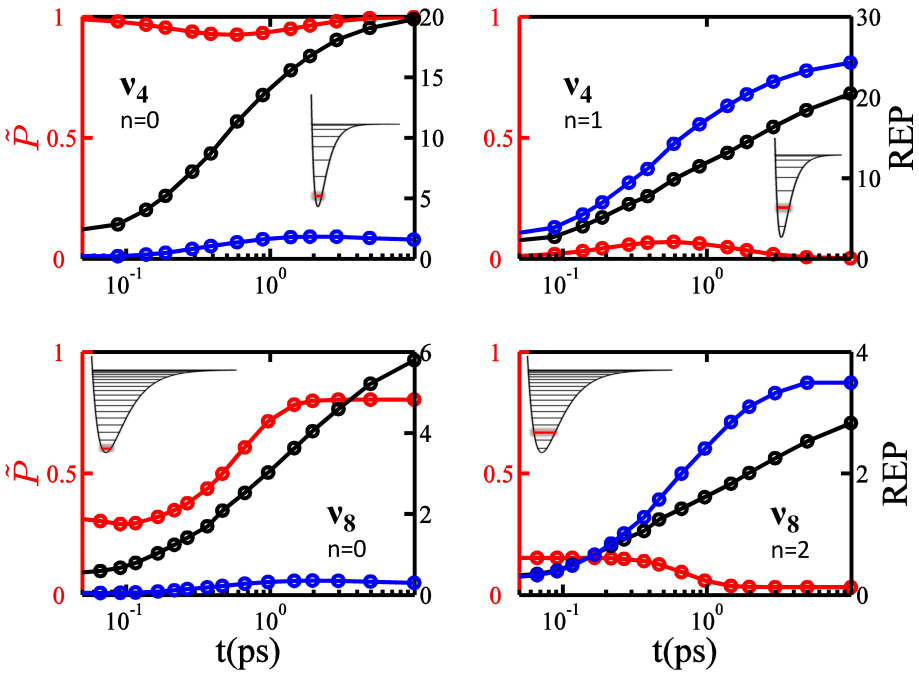

FIG. S3: **REP and occupation probability profiles.** Temporal profiles of REP (black and blue for RP at 440 nm and 460 nm, respectively) and vibrational population for a specific level, n, of a given mode (red, normalised to the total population $\tilde{P}_{i,n} = \frac{P_{i,n}}{\sum_n P_{i,n}}$).

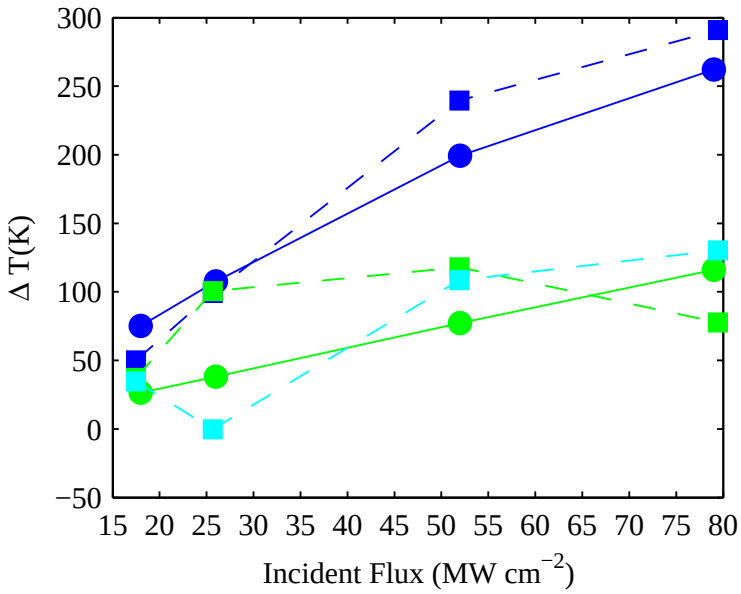

FIG. S4: **Temperature profiles: TRRS vs FSRRS.** Squares are TRRS data from Ref.[6], for ν_4 (blue line), ν_7 (green line) and ν_{CH} (cyan line). Circles are derived by our FSRRS study (as detailed in Supplementary Information) for a low frequency mode (ν_8, green line) and a high frequency mode (ν_4, blue line).

1. Petrich, J. W., Martin, J. L., Houde, D., Poyart, C. & Orszag, A. Time-resolved raman spectroscopy with subpicosecond resolution: vibrational cooling and delocalization of strain energy in photodissociated (carbonmonoxy)hemoglobin. *Biochemistry* **26**, 7914–7923 (1987).
2. Ye, X. *et al.* Investigations of heme protein absorption line shapes, vibrational relaxation, and resonance raman scattering on ultrafast time scales. *The Journal of Physical Chemistry A* **107**, 8156–8165 (2003).
3. Schomacker, K. T., Bangcharoenpaurpong, O. & Champion, P. M. Investigations of the stokes and antistokes resonance raman scattering of cytochrome c. *The Journal of Chemical Physics* **80**, 4701–4717 (1984).
4. Stallard, B. R., Champion, P. M., Callis, P. R. & Albrecht, A. C. Advances in calculating raman excitation profiles by means of the transform theory. *The Journal of Chemical Physics* **78**, 712–722 (1983).
5. Shim, S., Stuart, C. M. & Mathies, R. A. Resonance raman cross-sections and vibronic analysis of rhodamine 6G from broadband stimulated raman spectroscopy. *ChemPhysChem* **9**, 697–699 (2008).
6. Loparo, J. J., Cheatum, C. M., Ondrias, M. R. & Simpson, M. Transient raman observations of heme vibrational dynamics in five-coordinate iron porphyrins. *Chemical Physics* **286**, 353–374 (2003).
7. Li, P., Sage, J. T. & Champion, P. M. Probing picosecond processes with nanosecond lasers: Electronic and vibrational relaxation dynamics of heme proteins. *J. Chem. Phys.* **97**, 3214–3227 (1992).